LARGE-EDDY SIMULATION OF SCALAR DISPERSION FROM A POINT SOURCE OVER A WAVY WALL

David A. Philips
Department of Mechancial Engineering
Stanford University
Stanford, CA 94305
dphilips@stanford.edu

Riccardo Rossi
CTFD-Lab
Seconda Facoltà di Ingegneria di Forlì
Università degli Studi di Bologna
Via Fontanelle 40, 47121 Forlì, Italy

Gianluca Iaccarino
Department of Mechancial Engineering
Stanford University
Stanford, CA 94305

ABSTRACT

A Large-Eddy Simulation (LES) of scalar dispersion over a wavy wall has been performed and is compared with Direct Numerical Simulation (DNS) data for the same case. LES statistics show excellent agreement with DNS data at a much lower computational cost. The LES mesh cell count has been reduced by a factor of eight and the timestep doubled as compared to the DNS calculation. Mean flow and Reynolds stress data is presented along with mean scalar and scalar flux statistics. Barycentric maps are used to visualize the state of turbulence in the flow field captured by LES while scatter plots of mean scalar concentration give an overall picture of predictive performance. For both of the prior analysis techniques, RANS results are included in the discussion to place the LES results in appropriate context in terms of computational expense and accuracy.

INTRODUCTION

From tracking the spread of the release of a hazardous material to predicting the impact on air quality due to emissions, there are many important applications for scalar dispersion modeling. The high population densities found in urban areas make them important regions in which dispersion must be understood (Britter and Hanna, 2003). The complex geometries found in urban areas pose an additional modeling challenge. With the advent of automated unstructured meshing techniques, Computational Fluid Dynamics (CFD) methods are suited for scales at which individual buildings must be resolved. Comparisons of Reynolds-Average Navier Stokes (RANS) and Large-Eddy Simulation (LES) approaches to dispersion modeling are still common in the literature for both real urban areas (Gousseau et al., 2011) and idealized geometries (Salim et al., 2011) as the best method is still up for debate (Fernando et al., 2010).

This LES study builds upon prior investigations of dispersion (Rossi et al., 2010; Rossi, 2010; Philips et al., 2010) in which various RANS methodologies were explored. RANS simulations in complex geometries were found to yield reasonable results when the turbulence models effectively captured anisotropies in the Reynolds stresses. Additionally, a scalar flux model that takes advantage of this anisotropy information is required. The Standard Gradient Diffusion Hypothesis (SGDH) uses a scalar value for the diffusivity that does not always capture the correct behavior of the turbulent scalar flux. Tensorial formulations of the diffusivity are better suited to incorporate flow anisotropy information in the scalar field prediction. In the current work, the anisotropy in the turbulent flow predicted by LES will be examined. If the modeled subgrid stresses and fluxes are truly isotropic, then large scale anisotropy should be captured without the need for the type of models employed in the RANS approach.

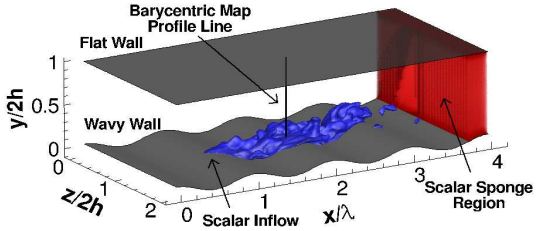

Figure 1: Computational domain

NUMERICAL EXPERIMENT

An LES of fully developed turbulent flow through a wavy channel is performed at a Reynolds number of approximately $6,800$ based on the mean channel height, $2h$, and the bulk velocity. A passive scalar with a Schmidt number, $Sc = 1$, is released from the wave crest and allowed to develop downstream. The accuracy of this LES study will be assessed via comparison with DNS data presented and analyzed in

Rossi and Iaccarino (2009). Additionally, RANS modeling results from Philips et al. (2010) are discussed to further contextualize the results of this study.

Governing Equations

The filtered continuity, momentum, and passive scalar transport equations,

$$\frac{\partial \bar{U}_i}{\partial x_i} = 0 \tag{1}$$

$$\frac{\partial \bar{U}_i}{\partial t} + \frac{\partial \bar{U}_i \bar{U}_j}{\partial x_j} = -\frac{1}{\rho}\frac{\partial \bar{p}}{\partial x_j} + \nu \frac{\partial \bar{U}_i}{\partial x_j \partial x_j} - \frac{\partial \tau^r_{ij}}{\partial x_j} + \frac{1}{\rho}\Pi_g \tag{2}$$

$$\frac{\partial \bar{C}}{\partial t} + \frac{\partial \bar{C}\bar{U}_j}{\partial x_j} = \frac{\nu}{Sc}\frac{\partial \bar{C}}{\partial x_j \partial x_j} - \frac{\partial q_j}{\partial x_j} - \Phi_{sp} \tag{3}$$

are solved using the unstructured, finite volume code CDP developed at Stanford's Center for Turbulence Research. A semi-implicit Crank-Nicholson method is used to advance the solution in time while centered differencing is used for spatial derivatives. The dynamic Smagorinski model of Germano et al. (1991) was used to close the subgrid stresses, τ^r_{ij}, in the momentum equation. A constant turbulent Schmidt number, $Sc_t = 0.9$, was then used to obtain the subgird scalar fluxes, q_j. Further details on CDP may be found in Mahesh et al. (2004); Ham and Iaccarino (2004); Ham et al. (2006).

Computational Domain and Mesh

The wavy wall computational domain is shown in Fig. 1 where the wavelength, λ, is set equal to $2h$. A fully developed turbulent flow is driven by a constant pressure gradient applied as a source term, Π_g, to the x-momentum equation. While the flow is periodic in the streamwise, x, and spanwise, z, directions, the scalar field is not. The scalar develops for approximately three wavelengths before being removed from the domain via a sponge. The sponge term Φ_{sp}, shown in Eq. 3, is active only in the region $x/\lambda = 3.75$ to $x/\lambda = 4.00$ but there may be effects on the scalar field immediately upstream due to recirculating turbulent eddies. All analysis is therefore performed well upstream of the sponge region.

The details of the computational mesh for the aforementioned geometry are shown in Tbl. 1. The number of computational cells used in each direction for the LES was half that for the DNS except in the spanwise direction where an odd number was necessary to maintain the same source position. The characteristic velocity,

$$U_* = \left(\frac{2h\Pi_g}{\rho}\right)^{1/2} \tag{4}$$

is defined based on the imposed pressure gradient Π_g and the channel height. This velocity scale is used to define the mesh plus-spacing values reported in Tbl. 1.

Simulation Procedure

The simulation was initialized and advanced in time for approximately $80T$ to remove initial transients, where T is one flow through time. The flow and scalar field was then monitored and averaged over approximately $350T$ using a timestep of $1.75T \times 10^{-3}$. Flow field statistics presented hereafter will be normalized by U_*, while scalar field statistics will be normalized by the concentration at the source, C_0. Angled brackets, $\langle\rangle$, will be used to designate time averaged quantities, to differentiate from the overbar used for the filtering operation. Note that though the filtering overbar is omitted on comparison plots, the statistics presented for the LES computation are time averages of resolved quantities, while the DNS statistics presented have not been filtered.

Table 1: Wavy wall mesh parameters

CASE	$N_x \times N_y \times N_z$	$\Delta x^+ \times \Delta y^+ \times \Delta z^+$
DNS	$256 \times 96 \times 128$	$14 \times 0.13 - 18 \times 14$
LES	$128 \times 48 \times 65$	$27 \times 0.70 - 37 \times 27$

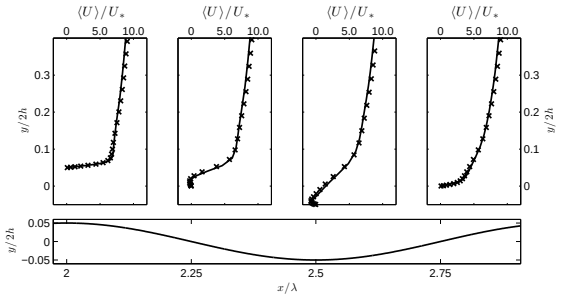

Figure 2: Vertical profiles of mean streamwise velocity: × DNS, — LES resolved

FLOW FIELD PREDICTION

Mean Flow

Profiles of mean velocity in the streamwise direction are shown in Fig. 2 and the LES is found in excellent agreement with DNS data at the four streamwise stations shown. The mean velocity is under-predicted very slightly towards the channel center, but the separated and reattached flow regions near the wall are predicted well. The mean vertical velocity is also predicted well by LES, though the profiles are omitted here for the sake of brevity.

Reynolds Stresses in Physical Space

The Reynolds stresses predicted by the LES computation are now compared with DNS data. The resolved shear stress, $\langle u'v' \rangle$, is well represented up to $y/2h \approx 0.15$ at which point the predicted magnitude is larger than DNS (Fig. 3). Additionally, the peak shear stress in the separated downslope region is somewhat greater than found in the DNS case. The subgrid shear stress predicted by LES is reported in Fig 3 along with the resolved shear stress to illustrate the modeling contribution. At maximum, the subgrid shear stress was 5% to 6% of the resolved stress on the wave downslope and trough, respectively. Given the small difference, only the resolved stresses

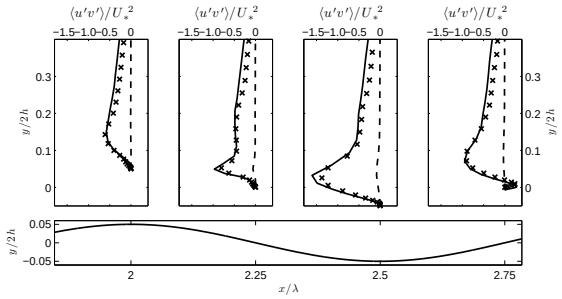

Figure 3: Vertical profiles of the $\langle u'v' \rangle$ Reynolds stress: $\times$ DNS, — LES resolved, - - - LES subgrid

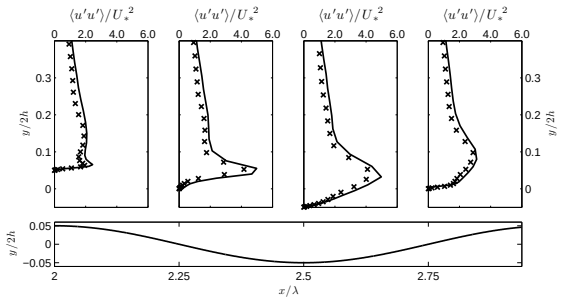

Figure 4: Vertical profiles of the $\langle u'u' \rangle$ Reynolds stress: $\times$ DNS, — LES resolved

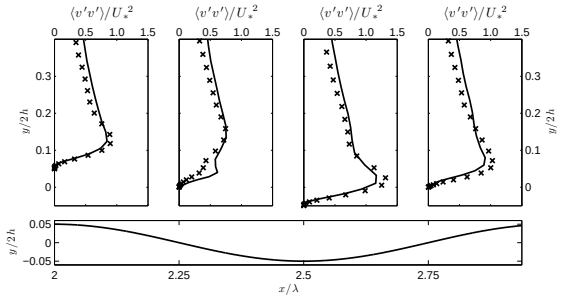

Figure 5: Vertical profiles of the $\langle v'v' \rangle$ Reynolds stress: $\times$ DNS, — LES resolved

are reported subsequently for the normal Reynolds stress components. The shape of the $\langle u'u' \rangle$ stress matches qualitatively with DNS data, though its magnitude is slightly over predicted by LES (Fig. 4). Nevertheless, the height of the profile peak at each location is consistent with DNS. In the separated flow region at $x/\lambda = 2.25$, the $\langle v'v' \rangle$ stress profiles contains a peak at $y/2h \approx 0.05$ that is not as prominent in the DNS data (Fig. 5). At the other streamwise locations, LES under-predicts the peak value of the $\langle v'v' \rangle$ stress but slightly over-predicts the values in the channel center. Like the $\langle v'v' \rangle$ stress, $\langle w'w' \rangle$ is also over-predicted by LES towards the center of the channel (Fig. 6). The near-wall peak in the $\langle w'w' \rangle$ stress is captured accurately by the LES on the wave upslope; however, the development of this peak, as seen in the wave trough profile, begins earlier than in the DNS data.

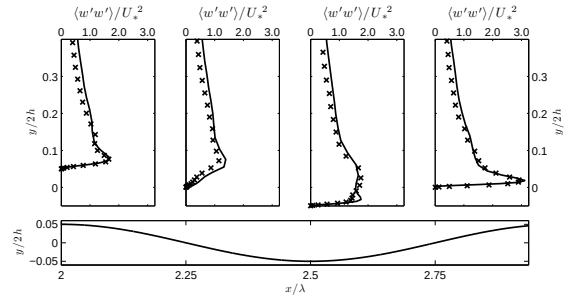

Figure 6: Vertical profiles of the $\langle w'w' \rangle$ Reynolds stress: $\times$ DNS, — LES resolved

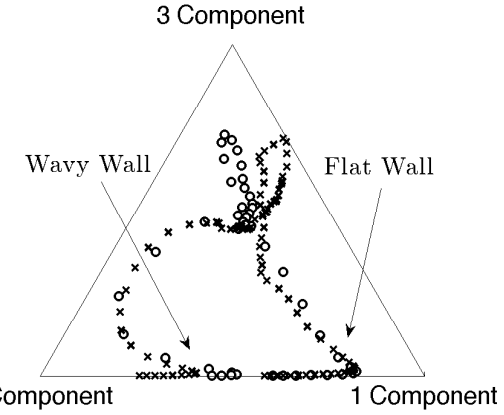

Figure 7: Barycentric map for a vertical profile at the wave crest: $\times$ DNS, $\circ$ LES resolved

Barycentric Map Analysis

Further analysis of the turbulent flow field is now performed using the Barycentric mapping method of Banerjee et al. (2007). The method is similar to the invariant approach of Lumley and Newman (1977) except that a linear mapping is used to create the barycentric triangle shown in Fig. 7. The corners of the triangle represent the one, two, and three component states of turbulence which is equivalent to the number of zero eigenvalues of the Reynolds stress tensor, $\left\langle u_i' u_j' \right\rangle$. The state of turbulence along a vertical profile at the wave crest, indicated in Fig. 1, is plotted in Fig. 7 for both the DNS data and LES prediction. The results show excellent agreement in predicting the peak towards one-component turbulence along the flat wall. The peak corresponds to a maximum in turbulence production and the effectiveness of LES in capturing this peak fits well with the idea that it resolves the large scale features of the flow. The one-component peak near the wavy wall side of the channel is shifted more towards two-component turbulence and there is a greater difference in the prediction of LES versus DNS. Recalling the plots of the Reynolds stresses in physical space at the wave crest, $\langle u'u' \rangle$ was over-predicted in the near-wall region, while the magnitudes of $\langle v'v' \rangle$ and $\langle u'v' \rangle$ were under-predicted suggesting a slightly more one-component nature. Lastly, the state of turbulence near the center of the channel shows the LES data shifted to be more in line with isotropic (three-component)

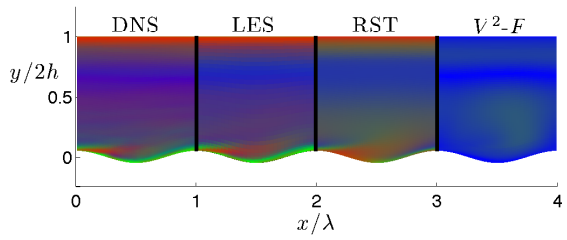

Figure 8: Barycentric colormap in physical space. Red / Green / Blue : 1 / 2 / 3 component turbulence, respectively

turbulence. Therefore, some anisotropy information in the resolved stresses has been lost due to the reduction in grid resolution and the subgrid modeling. To put this move towards isotropy in context, it is instructive to compare the state of turbulence captured by DNS and LES to RANS modeling formulations. Fig. 8 shows the wavy wall physical domain filled with a colormap representing location within the barycentric triangle mapping. Given the periodic nature of the flow, four results are displayed side by side. Comparing the DNS and LES sections of Fig. 8, a slight smoothing of the colormap is noticeable particularly in the channel center where the flow becomes slightly more isotropic (blue). The first RANS method shown is a second moment closure Reynolds Stress Transport (RST) method (Launder, B. E. et al., 1975). By solving transport equations for the six independent Reynolds stresses it captures some of the basic turbulence structure but the colormap shows clear variations from that of the DNS. Still other RANS approaches like the v^2-f model (Durbin, 1991) shown furthest to the right in Fig. 8 use the Boussinesq approximation to calculate the stresses which leads to a more isotropic prediction of the state of turbulence. While a similar approximation is used for the LES subgrid stresses, it is clear from the colormap that this does not significantly change the predicted turbulence anisotropy of the large scales as compared with DNS. Further details of the RANS approach may be found in Philips et al. (2010).

SCALAR FIELD PREDICTION

Mean Scalar

Results for the LES computation of mean scalar concentration are shown in Figs. 9 and 10. The shape of the vertical profiles shown in Fig. 9 is captured effectively by LES, though the magnitude is under-predicted. The greatest deviation occurs on the wave downslope where there is a peak in scalar concentration at approximately $y/2h = 0.05$. Recall that in this region the flow is separated and the Reynolds stresses were slightly over-predicted. The increased turbulent mixing leads to a lower value of scalar concentration predicted by LES as compared to DNS. Spanwise profiles of mean concentration are reported in Fig. 10. Again, LES generally underpredicts the concentration. While this is apparent at the center of the plume, $z/2h = 1$, the LES agrees quite well with DNS data towards the edge of the plume beginning around $z/2h = 0.85$.

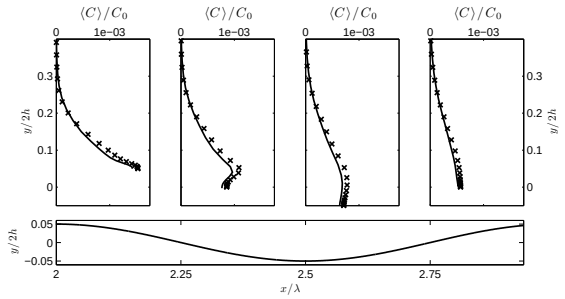

Figure 9: Vertical profiles of mean scalar concentration: $\times$ DNS, — LES resolved

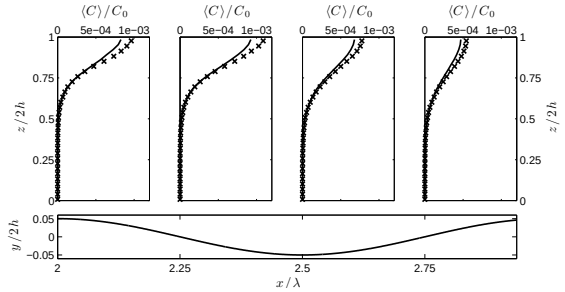

Figure 10: Spanwise profiles of mean scalar concentration at $y/2h = 0.05$ above the wavy wall surface: $\times$ DNS, — LES resolved

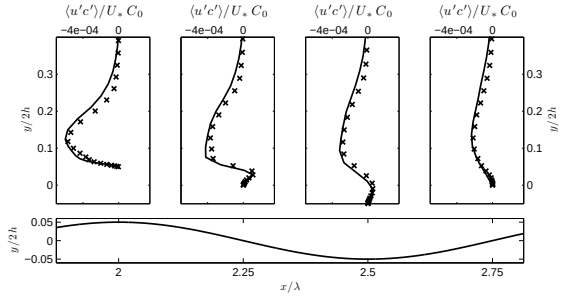

Figure 11: Vertical profiles of streamwise scalar flux: $\times$ DNS, — LES resolved

Scalar Flux

The resolved turbulent scalar fluxes from LES are reported in this section. The contribution of the modeled subgrid fluxes was small with a maximum of 2.5% of the resolved component, and as such they are not shown here for the sake of brevity. Vertical profiles of the streamwise flux in Fig. 11 show that the LES yields a reasonable representation though the extent of the negative peak is slightly broader as compared with DNS data. Agreement in the near-wall region is excellent as the location and magnitude of the positive peak is well captured. As seen in Fig. 12, the peak value of the vertical flux is under-predicted at the wave crest but agreement improves moving downstream. A spanwise plot is included to show the behavior of the spanwise flux (Fig. 13). LES predicts a much broader peak in spanwise flux on the wave downslope than the

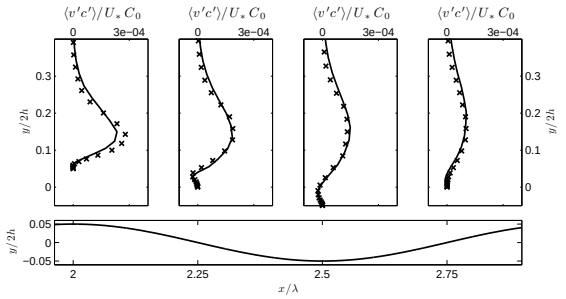

Figure 12: Vertical profiles of vertical scalar flux: × DNS, — LES resolved

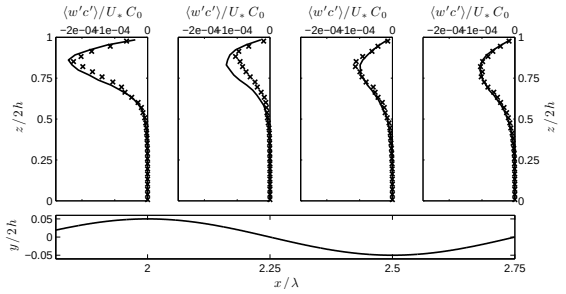

Figure 13: Spanwise profiles of spanwise flux at $y/2h = 0.05$ above the wavy wall surface: × DNS, — LES resolved

DNS data indicates. Despite this disagreement upstream, the spanwise flux is well represented in the wave trough and wave upslope.

Scatter Data Analysis

Much as the barycentric colormap in Fig. 8 allowed for greater analysis of the state of turbulence, the scatter plots of mean concentration presented herein provide a look at the overall predictive performance. Fig. 14 takes the mean concentration data from the DNS dataset and plots it versus a LES or RANS prediction at the same point. In the case of a perfect model, all data points would lie along the solid black line shown in Fig. 14. Deviation from the central black line indicates error in the predicted mean scalar values and the dashed black lines delimit one decade of over-prediction or under-prediction. As can be seen in the first plot of Fig. 14, the LES simulation is not biased towards over or under-prediction and remains well within an order of magnitude of the DNS data down to a concentration of $\langle C/C_0 \rangle \approx 10^{-6}$. The bottom two plots of Fig. 14 are included to show results typical of a RANS approach for the current geometry. In this case, results are shown from the v^2-f model using two different models for the turbulent diffusivity. The Standard Gradient Diffusion Hypothesis (SGDH) is a constant turbulent Schmidt number approach that leads to a bias towards under-prediction and large deviations from DNS data. The Generalized Gradient Diffusion Hypothesis (GGDH) is a tensorial formulation of the turbulent diffusivity proposed by Daly and Harlow (1970). It incorporates more flow anisotropy information, see Philips et al. (2010) for further details, and is successful in reducing the

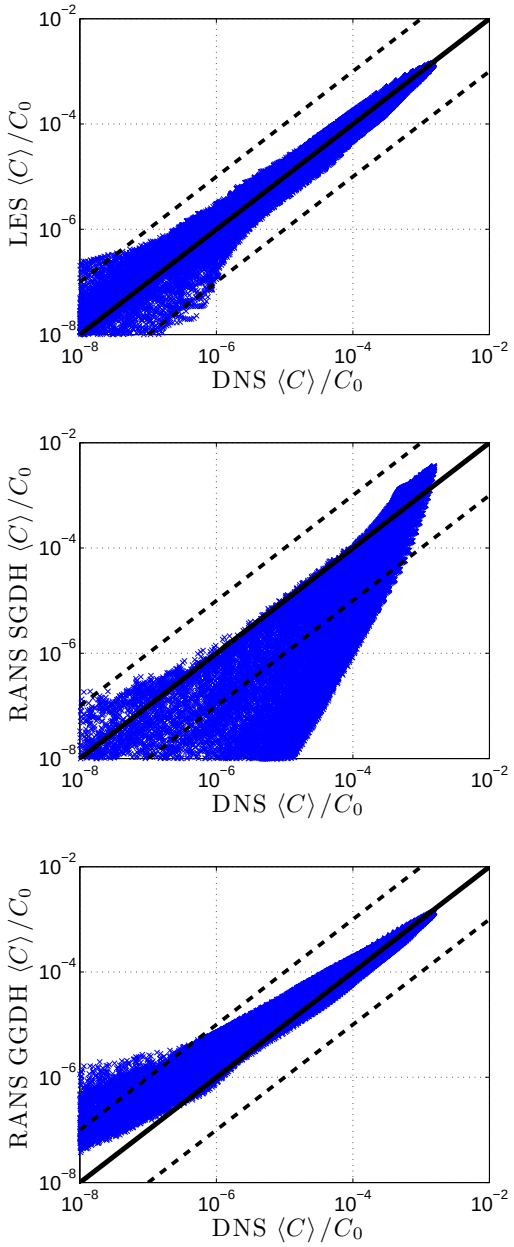

Figure 14: Scatter plots comparing DNS mean concentration values from the region $2 < x/\lambda < 3$ to modeled concentration values: top, LES; Middle, RANS SGDH; bottom, RANS GGDH

data spread; although, a modest bias towards over-prediction now occurs.

DISCUSSION

In this study, a LES of scalar dispersion through a wavy channel was performed. LES was effective in predicting scalar dispersion over the wavy wall. Differences in mean flow prediction between LES and DNS were extremely small. A barycentric analysis of the state of stress predicted by LES

indicated a slightly more isotropic turbulence in the center of the channel than the DNS case; however, the overall state was reproduced much more accurately than was obtained using RANS models. The LES mean scalar prediction was good, though not quite as accurate as the mean flow results. This could be related to the simplified, constant Sc_t approach taken to close the subgrid fluxes. A future evaluation should consider calculating this value dynamically. Nevertheless, scatter plots showed an unbiased overall predictive performance by the LES with minimal data spread from DNS values. While more sophisticated RANS approaches could reduce the spread in mean scalar prediction, a slight bias towards over or under-prediction remained. While the results herein generally indicate a stronger performance by LES than RANS, simulation cost must be taken into account. The RANS calculations discussed can be performed over a period of several hours while collecting statistics from the LES took on the order of days. Moving to higher Reynolds numbers is another necessity, as the quality of the LES results may decrease as the subgrid modeling contribution to the solution increases. Nevertheless, at higher Reynolds numbers, LES and RANS may continue to fulfill different roles with LES providing a baseline for improvement in RANS modeling.

Acknowledgements

The authors acknowledge the following award for providing computing resources that have contributed to the research results reported within this paper: MRI-R2, Acquisition of a Hybrid CPU/GPU and Visualization Cluster for Multidisciplinary Studies in Transport Physics with Uncertainty Quantification. This award is funded under the American Recovery and Reinvestment Act of 2009 (Public Law 111-5)

REFERENCES

S. Banerjee, R. Krahl, F. Durst, and C. Zenger, "Presentation of anisotropy properties of turbulence, invariants versus eigenvalue approaches," *Journal of Turbulence*, vol. 8, no. N32, 2007.

R. E. Britter and S. R. Hanna, "Flow and dispersion in urban areas," *Annual Review of Fluid Mechanics*, vol. 35, no. 1, pp. 469–496, 2003.

B. J. Daly and F. H. Harlow, "Transport equations in turbulence," *Physics of Fluids*, vol. 13, no. 11, pp. 2634–2649, 1970.

P. A. Durbin, "Near-wall turbulence closure modeling without damping functions," *Theoretical and Computational Fluid Dynamics*, vol. 3, pp. 1–13, 1991.

H. J. S. Fernando, D. Zajic, S. D. Sabatino, R. Dimitrova, B. Hedquist, and A. Dallman, "Flow, turbulence, and pollutant dispersion in urban atmospheres," *Physics of Fluids*, vol. 22, no. 5, p. 051301, 2010.

M. Germano, U. Piomelli, P. Moin, and W. H. Cabot, "A dynamic subgrid-scale eddy viscosity model," *Physics of Fluids A: Fluid Dynamics*, vol. 3, no. 7, pp. 1760–1765, 1991.

P. Gousseau, B. Blocken, T. Stathopoulos, and G. van Heijst, "CFD simulation of near-field pollutant dispersion on a high-resolution grid: A case study by LES and RANS for a building group in downtown montreal," *Atmospheric Environment*, vol. 45, no. 2, pp. 428 – 438, 2011.

F. Ham and G. Iaccarino, "Energy conservation in collocated discretization schemes on unstructured meshes," Center for Turbulence Research, Annual Research Briefs, pp. 3–14, 2004.

F. Ham, K. Mattsson, and G. Iaccarino, "Accurate and stable finite volume operators for unstructured flow solvers," Center for Turbulence Research, Annual Research Briefs, pp. 243–261, 2006.

Launder, B. E., Reece, G. J., and Rodi, W., "Progress in the development of a reynolds-stress turbulence closure," *Journal of Fluid Mechanics*, vol. 68, no. 03, pp. 537–566, 1975.

J. L. Lumley and G. R. Newman, "The return to isotropy of homogeneous turbulence," *Journal of Fluid Mechanics*, vol. 82, no. 01, pp. 161–178, 1977.

K. Mahesh, G. Constantinescu, and P. Moin, "A numerical method for large-eddy simulation in complex geometries," *Journal of Computational Physics*, vol. 197, no. 1, pp. 215 – 240, 2004.

D. A. Philips, R. Rossi, and G. Iaccarino, "The influence of normal stress anisotropy in predicting scalar dispersion with the v^2-f model," Stanford University, Tech. Rep., 2010, submitted.

R. Rossi, "A numerical study of algebraic flux models for heat and mass transport simulation in complex flows," *International Journal of Heat and Mass Transfer*, vol. 53, no. 21-22, pp. 4511 – 4524, 2010.

R. Rossi and G. Iaccarino, "Numerical simulation of scalar mixing from a point source over a wavy wall," Center for Turbulence Research, Annual Research Briefs, pp. 453–464, 2009.

R. Rossi, D. Philips, and G. Iaccarino, "A numerical study of scalar dispersion downstream of a wall-mounted cube using direct simulations and algebraic flux models," *International Journal of Heat and Fluid Flow*, vol. 31, no. 5, pp. 805 – 819, 2010.

S. M. Salim, R. Buccolieri, A. Chan, and S. D. Sabatino, "Numerical simulation of atmospheric pollutant dispersion in an urban street canyon: Comparison between RANS and LES," *Journal of Wind Engineering and Industrial Aerodynamics*, vol. 99, no. 2-3, pp. 103 – 113, 2011.